JOURNAL OF GUIDANCE, CONTROL, AND DYNAMICS
Vol. 18, No. 6, November–December 1995

Near-Minimum-Time Maneuvers of Large Structures: Theory and Experiments

S. R. Vadali,* M. T. Carter,† and T. Singh‡
Texas A&M University, College Station, Texas 77843-3141
and
N. S. Abhyankar§
Dynacs Engineering Company, Clearwater, Florida 34621-2596

This paper describes the design and implementation of near-minimum-time control laws for the Advance Space Structures Technology Research Experiments test article located at the Phillips Laboratory, Edwards Air Force Base. The test article is equipped with compressed air thrusters that can be throttled. The mathematical model of the rotational motion is obtained by using experimental data and includes effects such as thruster dynamics, fuel constraints, leakage, and multibody interactions. Both open-loop and feedback strategies are developed and verified experimentally. The open-loop thruster profiles are generated using constrained parameter optimization. The feedback control profiles are generated using Lyapunov stability theory, for both final position regulation and tracking of the open-loop commands. The results show excellent agreement between theory and experiment.

Introduction

OPTIMAL large-angle maneuvering of spacecraft has been a topic of interest for more than two decades.[1,2] Many current and future spacecraft require rapid large-angle maneuvering with vibration suppression during and after maneuvers. The Phillips Laboratory at the Edwards Air Force Base has developed the Advanced Space Structures Technology Research Experiments (ASTREX) facility to serve as a testbed for demonstrating the applicability of proven theories to the challenges of spacecraft maneuvers and structural control.[3] This paper presents the control design methods for maneuvering the test article and experimental results obtained under the NASA/DOD Control-Structure Interaction (CSI) Guest Investigator Program.

In this paper, near-minimum-time, large-angle maneuvers of structures using throttlable compressed air thrusters are considered. The specific structure under consideration is schematically represented in Fig. 1. The connection of the primary structure to the support pedestal with a slight center of gravity (c.g.) offset from the pivot point resulted in a very low frequency pendulum mode at approximately 0.05 Hz. Controlling this mode was one of the objectives of this work.

The thruster orientation gives rise to significant interaxis coupling. To reduce the complexity of the control laws, designs of the control inputs were based on a rigid-body model, but torque smoothing was used to minimize high-frequency structural excitations. The open-loop thrust profiles were computed to optimize the switch times, maximum thrust magnitudes, and smoothing parameters, using the sequential quadratic programming (SQP) technique.[4] A maximum fuel consumption constraint was also included to account for limited fuel available to the thrusters. The effects of significant air leakage were also included. The feedback control profiles were generated using Lyapunov stability theory[5–8] for both final position regulation and tracking of the open-loop commands. Simulation results as well as experimental results are presented.

Received May 26, 1994; presented as Paper 94-3624 at the AIAA Guidance, Navigation, and Control Conference, Scottsdale, AZ, Aug. 1–3, 1994; revision received March 20, 1995; accepted for publication March 27, 1995.

*Professor, Department of Aerospace Engineering. Associate Fellow AIAA.
†Graduate Student, Department of Aerospace Engineering. Student Member AIAA.
‡Research Associate, Department of Aerospace Engineering; currently Assistant Professor, Department of Mechanical Engineering, State University of New York at Buffalo, Buffalo, NY 14222. Member AIAA.
§Project Engineer, on site at Phillips Laboratory, Kirtland Air Force Base, NM 87117-5776.

Description and Modeling of ASTREX Test Article

The ASTREX test article is designed to float on a 5-m pedestal using a two-axis airbearing system. Its mass is approximately[3] 4106 kg. The primary structure is a 5.5-m truss that supports the thrusters and the control moment gyroscopes (CMGs). The secondary structure houses a reaction wheel. This structure is attached to the primary structure with a tripod formation of three 5.1-m graphite epoxy tubes with embedded sensors and actuators for vibration suppression. The tertiary structure holds the electronics and power supply for the data acquisition and control system. The test article nominally rests at an attitude of 30-deg nose-down pitch (rotation about the local horizontal) and 0-deg roll (about the Z^b axis). There is a specified yaw orientation (rotation about the local vertical) that is the reference or 0 deg.

The real-time control and data acquisition computer (CDAC) acquires attitude and vibration data from the angular position encoders, the rate sensors, and linear accelerometers on the ASTREX structure and commands the thrusters using Matrix_X/Autocode software. The CDAC includes a Vax3100 workstation as a front end, an INTEL 80386/Weitek 3167-based parallel processor unit, and an

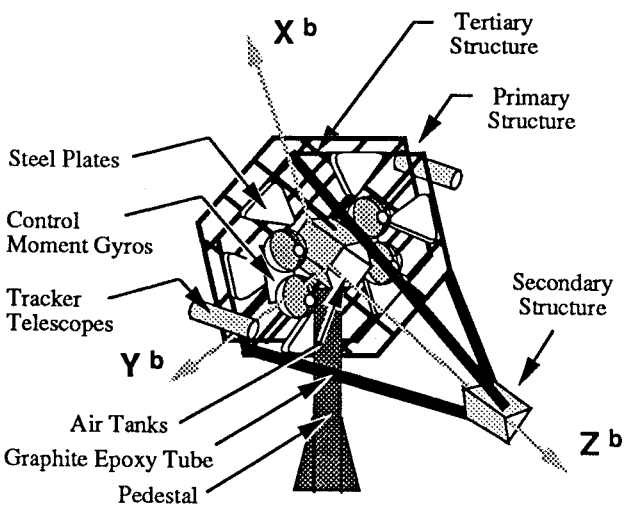

Fig. 1 Schematic of the ASTREX test article.

Table 1 Individual thruster location, positive voltage thrust direction, and saturation thrust

Bidirectional thruster no.	Node no.	Thurster location, m			+V thrust direction			Sat. thrust, lbf
		X^b	Y^b	Z^b	X^b	Y^b	Z^b	
1	327	−1.36581	−2.7116	−0.30839	0.500	0.0	0.867	8
2	325	1.33419	−2.7116	−0.30839	0.500	0.0	0.867	8
3	321	1.33419	2.7116	−0.30839	0.500	0.0	0.867	8
4	323	−1.36581	2.7116	−0.30839	0.500	0.0	0.867	8
5	427	−2.84230	0.0	−0.10658	0.0	1.0	0.0	8
6	437	2.81068	0.0	−0.10658	0.0	1.0	0.0	8
7 (7–8)	324	−1.36581	2.5465	−0.30839	0.500	0.0	0.867	200
8 (9–10)	322	1.33419	2.5465	−0.30839	0.500	0.0	0.867	200
9 (11–12)	328	−1.36581	−2.5465	−0.30839	0.500	0.0	0.867	200
10 (13–14)	326	1.33419	−2.5465	−0.30839	0.500	0.0	0.867	200

input/output unit having 32 input and 32 output channels for analog data as well as 64 bits of digital I/O.

The primary actuators are 14 thrusters located on the hexagonal primary structure. Of the 14 actuators, 6 are 8-lbf bidirectional thrusters and 8 are 200-lbf unidirectional thrusters. The 200-lbf thrusters are operated as four bidirectional thrusters. All of the thrusters can be throttled. These thrusters are canted so that they create moments about all of the three primary axes of the structure. The 8-lbf thrusters, on the average, have a bandwidth of 20 Hz, with a rise time of 9 ms and phase lag at 10 Hz of 17 deg. The 200-lbf thrusters have a bandwidth of 15 Hz, a rise time of 20 ms, and a phase lag of 25 deg at 10 Hz.

A NASTRAN finite element model[3] of the ASTREX test article is available. It consists of approximately 400 nodes and 900 elements. The first two structural modes at approximately 3.4 and 4.8 Hz are pedestal bending modes. The first bending mode of the truss structure is at 10.25 Hz. The data from this model are used to generate a linearized system description in the Matrix$_X$ SystemBuild environment. Control inputs, actuators, and sensors locations can be provided, and vibration and line-of-sight error estimates can be obtained using this model. For the present application, a rigid-body assumption is invoked for a preliminary control design due to the extreme separation between the control bandwidth and the structural modes. The approximate moment of inertia matrix with respect to the body coordinate system at the pivot point (units: kg-m^2) obtained from the finite element model is given as follows:

$$I = \begin{bmatrix} 18{,}941 & -25 & -243 \\ -25 & 11{,}804 & 25 \\ -243 & 25 & 14{,}188 \end{bmatrix}$$

The attitude is measured by angle encoding devices with a sensitivity of 3 μrad and is converted to quaternions (β) by the airbearing computer. The differential equation for the time rate of change of these parameters is given by

$$\dot{\beta} = \tfrac{1}{2} H^T(\beta)\omega \tag{1}$$

where

$$H(\beta) = \begin{bmatrix} -\beta_1 & \beta_0 & \beta_3 & -\beta_2 \\ -\beta_2 & -\beta_3 & \beta_0 & \beta_1 \\ -\beta_3 & \beta_2 & -\beta_1 & \beta_0 \end{bmatrix}$$

It is useful to write the preceding equation in its inverted form for estimating the angular velocities (ω) from quaternion measurements:

$$\omega = 2H(\beta)\dot{\beta} \tag{2}$$

The equation of rotational motion for a rigid body under the action of thrust moments only is

$$I\dot{\omega} = -\tilde{\omega} I\omega + B\boldsymbol{u} \tag{3}$$

where $\tilde{\omega}$ is the angular velocity cross product matrix, and B is the control influence matrix that depends on the maximum thrust of the individual thrusters as well as their moment arms. Hence the individual elements of $\boldsymbol{u}$ are bounded by ± 1. The thruster locations are given in Table 1 in the test article coordinate system shown in Fig. 1. The moment arms for the thrusters are obtained with respect to the pivot point from the preceding data. The thrusters are fired in pairs so as not to cause any translation. The six 8-lbf thrusters provide complete controllability of the test article; i.e., they provide independent moments along the three body axes. On the other hand, due to their orientation, the 200-lbf thrusters cannot completely control the test article and have to be augmented with the 8-lbf thrusters, nos. 5 and 6, to provide roll control. When a combination of the eight 200-lbf thrusters and the two 8-lbf roll thrusters is used,

$$B = \begin{bmatrix} 3924 & 3924 & 0 \\ -2080 & 2080 & 0 \\ -2265 & -2265 & 201.17 \end{bmatrix} \text{Nm}$$

All of the results presented in this paper are based on this choice for the thruster combination. It is also noted that thruster pair nos. 8(3–4) and 9(5–6) are commanded to provide nondimensional thrust magnitudes $u(1)$ and $-u(1)$, respectively. Thruster pair nos. 7(1–2) and 10(5–6) are commanded to provide $u(2)$ and $-u(2)$, respectively. The 8-lbf thrusters nos. 6 and 5 provide $u(3)$ and $-u(3)$, respectively.

To compute near-minimum-time open-loop maneuvers, it is necessary to impose a constraint on the maximum air volume available to the thrusters. The derivation of this constraint equation is presented in the next section.

Fuel Constraint

Two air tanks feed the thrusters in a blowdown manner. The capacity of each tank is 4 ft^3 with a maximum pressure of 500 psi. Assuming an isothermal expansion process, the volume of air available for the thrusters $v_{\max}$ at atmospheric pressure is related to the pressure drop ΔP in the tanks by the following equation:

$$v_{\max} = 8(\Delta P / P_{\text{at}})\ \text{ft}^3 \tag{4}$$

where P_{at} is the atmospheric pressure. Assuming a pressure drop of 250 psi, the air capacity at atmospheric pressure is estimated to be 136 ft^3. The air volume flow rate at atmospheric pressure v as specified by the manufacturer is given by the following relationship:

$$\dot{v} = 0.233 \left(\sum_{i=1}^{n} |T_i| \right) \frac{\text{ft}^3}{\text{s}} \tag{5}$$

where n is the number of thrusters and T_i is the thrust of each thruster. Equation (5) is integrated over the maneuver time to obtain the volume of air used, which is equivalent to the fuel consumed. Equation (4) is used to impose an inequality constraint on the volume of air available for the thrusters.

Open-Loop Command Generation Using Parameter Optimization

The maximum control magnitudes, switch times, and smoothing parameters subject to various constraints can be determined by solving a parameter optimization problem:

Minimize $J = (1/2)p_0^2$, subject to

$$\begin{aligned} \dot{\boldsymbol{x}} &= f[\boldsymbol{x}, \boldsymbol{u}(\boldsymbol{p}), \tau]p_0 \\ \boldsymbol{x}(1) &= \boldsymbol{x}_f \\ \boldsymbol{g}(p_i) &\geq 0 \\ p_{i_l} \leq p_i \leq p_{i_u} &\qquad i = 0, \ldots, n_p \end{aligned} \tag{6}$$

where p_0 is the final time and the various $\boldsymbol{p}$ are $n_p + 1$ parameters to be selected. The vector $\boldsymbol{p}$ includes the peak values of the three controls, the switch times, and the smoothing parameters. p_l and p_u are, respectively, the lower and upper bounds on the parameters. The state vector $\boldsymbol{x}$ consists of the quaternion, angular valocities, and the air volume at atmospheric pressure. The differential equations used in the optimization process include Eqs. (1), (3), and (5). Note that, for convenience, a nondimensional time τ is being used in Eq. (6), and therefore the final time is 1. This transformation of the time scale is affected by multiplying the right-hand sides of the differential equations by the parameter p_0. Since the four Euler parameters are not mutually independent, only the last three are constrained at the final time; β_0 is left free. Except for the air volume (fuel) and β_0, the prescribed state terminal boundary conditions are equality constraints. The fuel constraint is an inequality with $v_{\max}$ given by Eq. (4). The control saturation constraints and the constraints on the smoothing parameters are imposed directly using the parameter bounds. This is a general nonlinear programming problem. One way to solve this problem is through the use of sequential quadratic programming. Details of the formulations and examples are given in Ref. 4. The open-loop control and state profiles can be used to generate feedback laws using the Lyapunov approach as discussed in the next section.

Feedback Control

The application of Lyapunov stability to maneuver rigid and flexible spacecraft[5-7] has been demonstrated in many works. The unified framework for obtaining final position and tracking control laws using this procedure are summarized next.[5]

Let β_{ref}, ω_{ref}, and $\boldsymbol{u}_{\text{ref}}$, respectively, be the reference quaternion, the reference angular velocity, and the reference control profiles to be tracked. These quantities satisfy Eqs. (1) and (3). The reference profiles are generated using the open-loop approach discussed earlier. Then an error vector is created with respect to the current states as follows:

$$\begin{bmatrix} \boldsymbol{e}_\beta \\ \boldsymbol{e}_\omega \end{bmatrix} = \begin{bmatrix} \beta - \beta_{\text{ref}} \\ \omega - \omega_{\text{ref}} \end{bmatrix} \tag{7}$$

To drive this error to zero, a Lyapunov function V is defined as

$$V = k\boldsymbol{e}_\beta^T\boldsymbol{e}_\beta + \tfrac{1}{2}\boldsymbol{e}_\omega^T\boldsymbol{e}_\omega \tag{8}$$

where k is a positive scalar. The derivative of this function is

$$\dot{V} = \boldsymbol{e}_\omega^T\left[-kH(\beta)\beta_{\text{ref}} + I^{-1}(-\tilde{\omega}I\omega + B\boldsymbol{u}) - \dot{\omega}_{\text{ref}}\right] \tag{9}$$

The properties $H(\beta)\beta_{\text{ref}} = -H(\beta_{\text{ref}})\beta$ and $H(\beta)\beta = \boldsymbol{0}$ have been used to arrive at the preceding result.

The feedback control law can be derived as

$$\boldsymbol{u} = B^{-1}[I(kH(\beta)\beta_{\text{ref}} - k_1\boldsymbol{e}_\omega + \dot{\omega}_{\text{ref}}) + \tilde{\omega}I\omega] \tag{10}$$

where k_1 is a positive scalar. It is more practical to write the preceding equation as

$$\boldsymbol{u} = \boldsymbol{u}_{\text{ref}} + B^{-1}[I(kH(\beta)\beta_{\text{ref}} - k_1\boldsymbol{e}_\omega) + \tilde{\omega}I\omega - \tilde{\omega}_{\text{ref}}I\omega_{\text{ref}}] \tag{11}$$

The gains k and k_1 are selected to provide the required closed-loop natural frequency and damping ratio for a linearized model. The derivative of the Lyapunov function for the closed-loop system is of the following form:

$$\dot{V} = -k_1\boldsymbol{e}_\omega^T\boldsymbol{e}_\omega \tag{12}$$

It has been proven that the preceding control law renders $\dot{V}$ negative semidefinite. Further analysis using the Invariance Theorem assures the global asymptotic stability of the closed-loop system.[8,9] Simply put, when $\boldsymbol{e}_\omega$ is exactly zero, V achieves its global minimum only when $\boldsymbol{e}_\beta$ is exactly zero. This can be easily shown by taking the third derivative of V.

Before implementing the closed-loop control laws, the fidelity of the mathematical model was evaluated by using the open-loop control generated as discussed previously. Several improvements and modifications to the model were needed as a result of the preliminary experiments using the open-loop controls. Various unexpected problems and their accommodations are discussed in the next section.

Improvement of the Model Based on Experiments

Several important observations were made during the initial testing,[10,11] and these were used to improve the mathematical model of the system. They are listed as follows.

1) The inertia and c.g. offset data from the finite element model were not accurate enough. Hence, the c.g. offset was estimated experimentally, based on free oscillation tests. The frequency of the pendulum mode and the nominal equilibrium position of the test article were determined from these data. These frequencies were found to be 0.0455 Hz in roll and 0.0588 Hz in pitch. This c.g. location with respect to the pivot point was estimated as $\boldsymbol{r}_{cg} = [-0.02095,\ 0.00084,\ 0.01171]^T$ m. The test article does not have a unique yaw equilibrium state. It was found that the mean pitch equilibrium attitude is displaced approximately 0.8 deg from the estimated pitch resting position of 30 deg. The mean roll equilibrium position was approximately 0.23 deg.

2) Although the thrusters can be commanded with a maximum signal amplitude of 5 V, it was decided to limit the signal to ±4 V because of a problem with stray signals creeping in unexpectedly during tests. (Since then, the CDAC computer software has been updated to prevent accidental thruster firings.) This meant that the 200-lbf thrusters could be commanded for a maximum thrust of 100 lbf and the 8-lbf thrusters could be commanded for a maximum thrust of 4 lbf. The conversion factors are, approximately, 1 V = 1 lbf and 1 V = 30 psi pressure feedback for the 8-lbf thrusters. The conversion factors for the 200-lbf thrusters are, approximately, 1 V = 25 lbf and 1 V = 50 psi of pressure feedback.

3) Because of the blowdown nature of the tanks, the available air pressure drops with time when the thrusters are fired. Thrusters behave linearly for a pressure drop of about 100 psi starting with a tank pressure of nearly 480 psi. The typical starting tank pressure is approximately 480 psi. When the ball valves are opened to fill the nozzle chambers and tubing, the pressure drops to between 240 and 270 psi. Furthermore there is considerable leakage present. A leakage test was performed, and the results are given in Fig. 2. This phenomenon was modeled using a simple exponential fit of the data. An exponential fit was chosen so that the volume flow could be expressed as a linear differential equation.

4) The angular rate sensors mounted on the test article have a low-frequency cutoff of 1 Hz. Hence these are not reliable for obtaining rigid-body angular rate information. A digital rate estimator was designed to extract the angular rates by filtering the quaternion data. The filter was designed as two first-order filters in series—a pseudoderivative block with cutoff at 3.5 Hz and a low-pass filter with a cutoff at 12 Hz. The sampling interval was 0.004 s.

5) It is difficult to achieve the same initial attitude and air pressure for repeating experiments. Furthermore, each individual thruster has slightly different performance characteristics. It was observed that the 8-lbf thrusters generate more thrust than commanded and the 200-lbf thrusters have a time delay for sharp changes in the commanded thrust. The net change in the angular velocity during acceleration (initial pulse) was more than that during deceleration (second pulse) even though the thrust pulses had the same magnitude

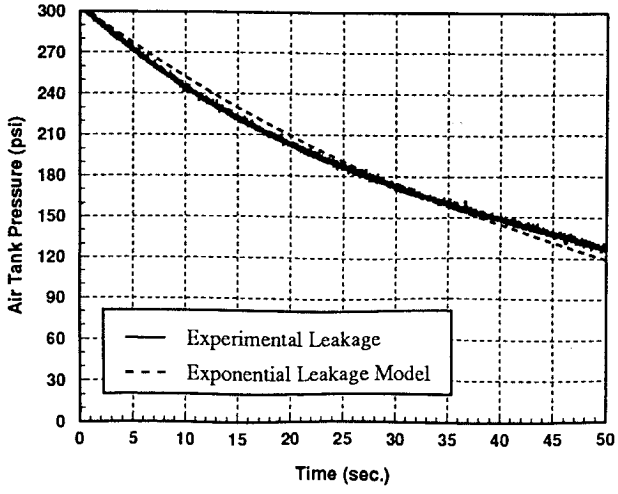

Fig. 2 Leakage test data.

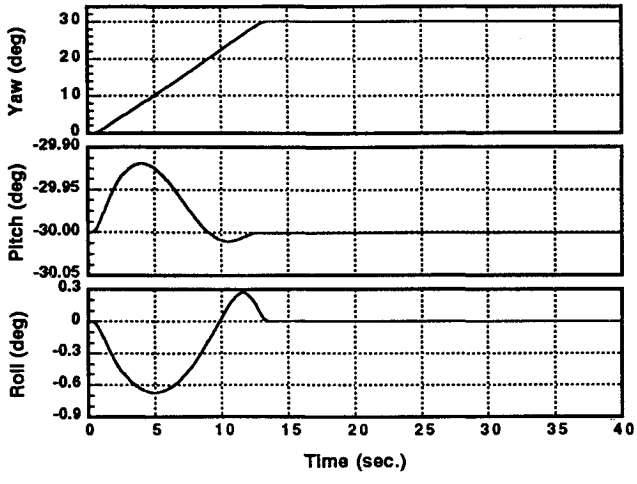

Fig. 3a Euler angles for the 30-deg open-loop yaw maneuver simulation.

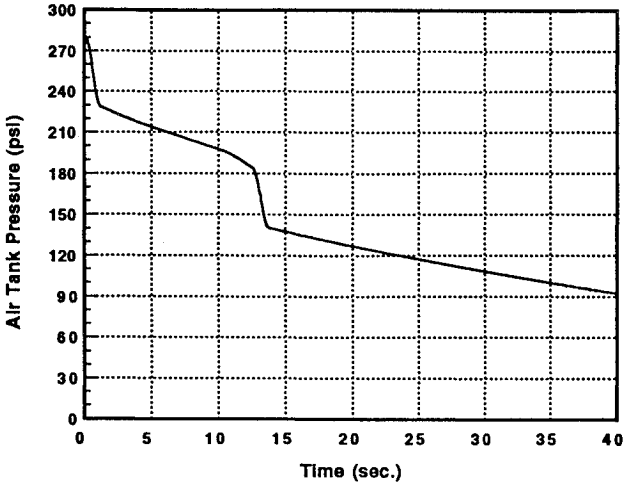

Fig. 3b Pressure drop for the 30-deg open-loop yaw maneuver simulation.

and width. This difference was attributed to unmodeled effects such as possible stiction. The actual thrust gain vector was determined by dividing the observed peak thrust by the simulated peak thrust for each thruster. These data were used to modify the B matrix in Eq. (3). Also worth noting is the fact that when the tank pressure dropped below 150 psi, the 8-lbf thruster responses were clipped for large thrust commands. The clipping effect was also observed for the 200-lbf thrusters when the pressure dropped below 30 psi.

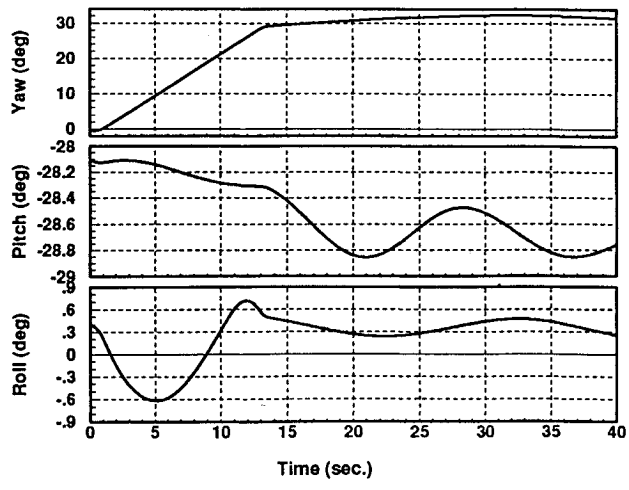

Fig. 4a Euler angles for the 30-deg open-loop yaw maneuver experiment.

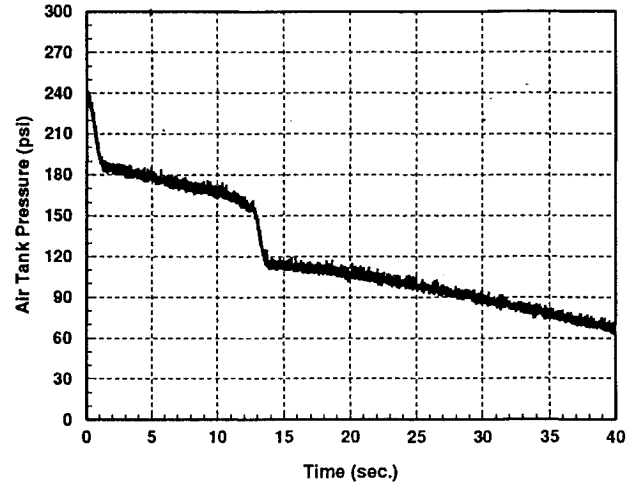

Fig. 4b Pressure drop for the 30-deg open-loop yaw maneuver experiment.

Based on the preceding observations, the following refined model was developed. Equation (5) was modified as shown next:

$$\dot{v} = 0.3081\left(\sum_{i=1}^{n}|T_i|\right) - 9.2\times 10^{-4}\left[\frac{P(0)}{P_{\text{at}}}\right]v \qquad (13)$$

where $P(0)$ is the initial tank pressure after the ball valve is opened and the thruster chambers are flooded.

Equation (3) was modified as follows:

$$I\dot{\omega} = -\tilde{\omega}I\omega + k_T B\boldsymbol{u} - Mg\tilde{r}_{cg}\begin{bmatrix} C_{11} \\ C_{21} \\ C_{31}\end{bmatrix} \qquad (14)$$

where k_T is a gain factor that is set to 0.85 during acceleration and 0.97 during deceleration for computing the open-loop command. These values were calculated for a starting position corresponding to the quaternion set [1, 0, 0, 0]. M is the mass of the test article and C is the direction cosine matrix. The first column of C is used in the preceding equation. Note that the gravity acts along the negative x direction of the inertial frame. The updated B matrix is given next:

$$B = \begin{bmatrix} 4022 & 3963 & 0.62 \\ -2144 & 2104 & 0 \\ -2322 & -2288 & 254,48\end{bmatrix}\ \text{Nm}$$

The open-loop and feedback control laws accounting for the modifications to the mathematical model are computed as discussed previously. The new B matrix is slightly different from its original

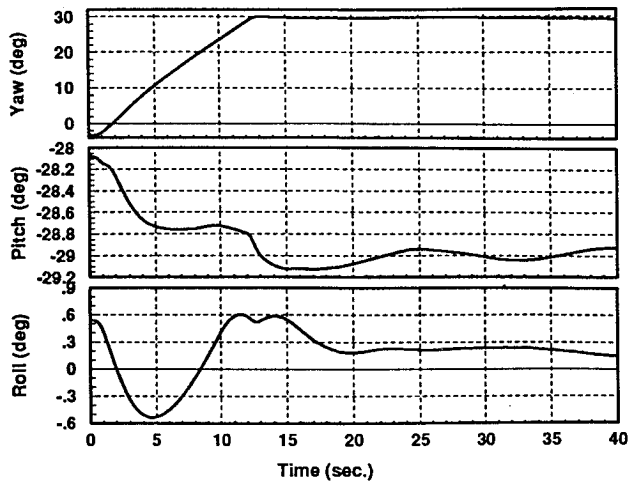

Fig. 5a Euler angles for the 30-deg closed-loop yaw maneuver experiment.

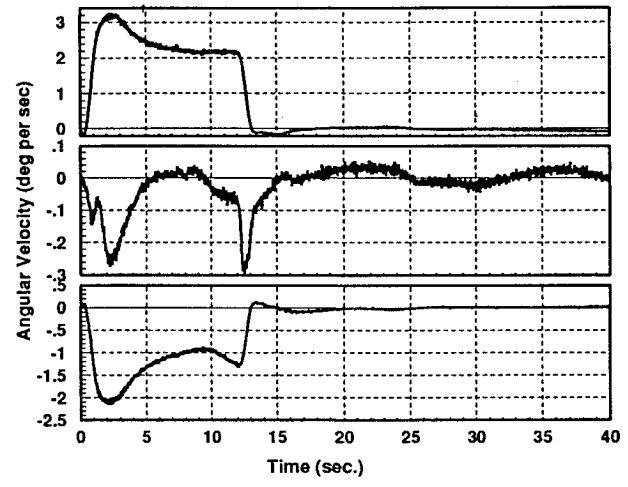

Fig. 5b Angular velocities for the 30-deg closed-loop yaw maneuver experiment.

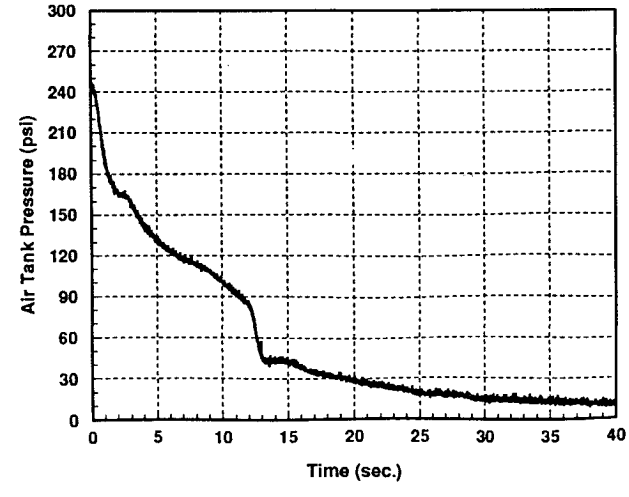

Fig. 5c Pressure drop for the 30-deg closed-loop yaw maneuver experiment.

version. The differences in the individual thruster characteristics give rise to an insignificant pivot point translation that has been neglected.

Results

Figures 3a and 3b show the results of a 30-deg open-loop yaw maneuver simulation. Figure 3a shows the Euler angles, and Fig. 3b shows the drop in tank pressure during the maneuver. This maneuver was constrained for a pressure drop of 140 psi with a starting pressure

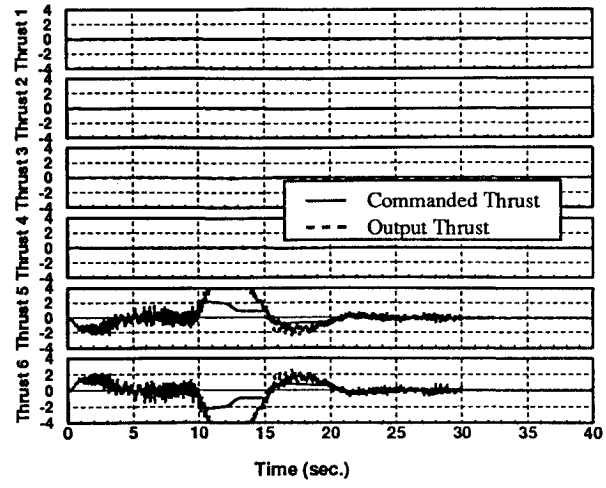

Fig. 6a Commanded and output thrust profiles for the 8-lbf thrusters.

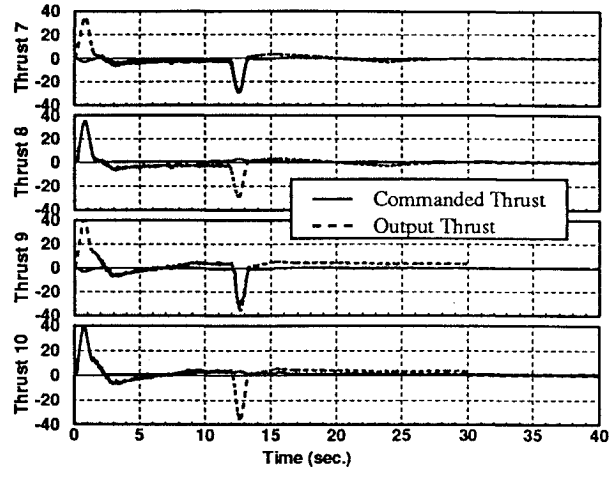

Fig. 6b Commanded and output thrust profiles for the 200-lbf thrusters.

of 280 psi. The maneuver time is approximately 14 s, although the simulation is extended to 40 s for later comparisons.

Figures 4a and 4b show the results of implementing the open-loop command. The initial attitude used in the simulation could not be matched exactly during the experiment, but the deviations are small. The yaw attitude is quite close to the desired value of 30 deg, but there is a slight amount of drift. The pitch axis attitude response shows a residual oscillation at approximately 0.05 Hz after the thrust is shut off at approximately 14 s. The roll axis attitude response also shows a slightly longer period residual oscillation. The starting pressure was 235 psi, and the pressure drop was approximately 110 psi at the end of the open-loop command.

Figures 5a–5c show the attitude, angular velocities, and the tank pressure, respectively, for a closed-loop tracking experiment. The gains k and k_1 in Eq. (11) were selected to provide a closed-loop natural frequency of 0.9 rad/s (0.14 Hz) and a damping ratio of 0.9 when operating in the linear region. The bandwidth was limited by the available air volume and pressure. The closed-loop control was applied only for 30 s. It is gratifying that the low-frequency oscillations found at the end of the open-loop maneuver (Fig. 4a) were nearly suppressed by the closed-loop controller and better performance would have been achieved had the initial pressure been higher. The initial tank pressure was 245 psi instead of the expected 280 psi.

Figures 6a and 6b show both the commanded (shown using dashed lines) and the output thrust profiles (shown using solid lines). The 8-lbf thrusters were commanded to saturate at 4 lbf. The output tracks the commanded thrust very well up to about 10 s. At this time the tank pressure was about 100 psi. After this time clipping is evident. The 200-lbf thrusters also fail to track the commanded input near the end of the open-loop command. A steady-state error near

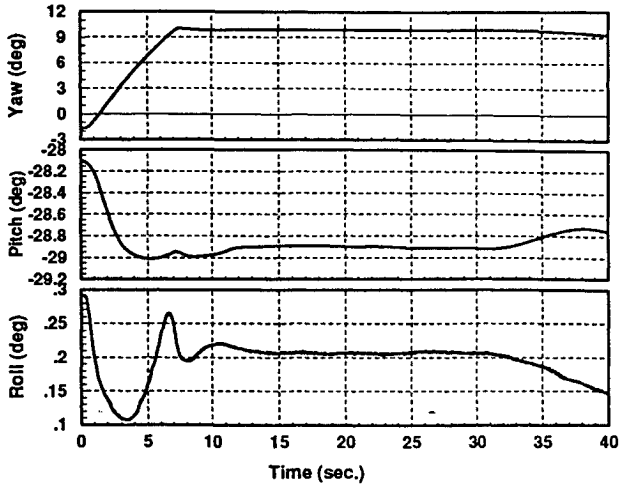

Fig. 7a Euler angles for the 10-deg closed-loop yaw maneuver experiment.

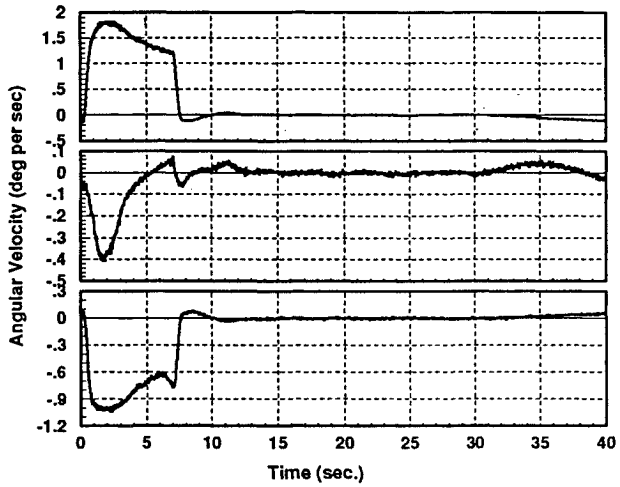

Fig. 7b Angular velocities for the 10-deg closed-loop yaw maneuver experiment.

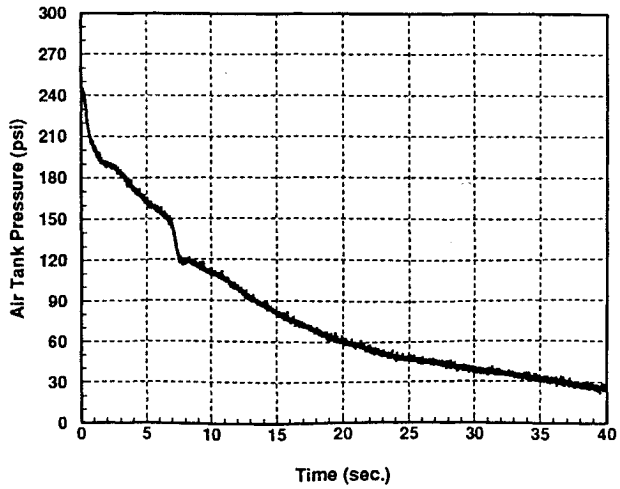

Fig. 7c Pressure drop for the 10-deg closed-loop yaw maneuver experiment.

the terminal region where the voltage command is too small for the thrusters to respond. With regard to Fig. 6b, it should be noted that, unlike the 8-lbf thrusters, the 200-lbf thrusters are unidirectional in terms of output thrust and a pair of them is used to produce a typical bang-off-bang profile. For example, thruster no. 7 can only produce negative thrust, whereas the required positive thrust is produced by thruster no. 8. While one thruster of a pair is firing, the pressure sensor of the other thruster outputs a signal as can be seen from Figs. 6b, but no thrust is produced by the inactive thruster. This was experimentally verified.

Figures 7a–7c show the effectiveness of the thrusters to suppress the low-frequency pendulum oscillations mentioned earlier when enough pressure is available. In this experiment, the test article was commanded to perform a 10-deg yaw maneuver. The open-loop command was computed as described earlier with an 85-psi pressure drop constraint and the closed-loop tracking controller was used. The yaw, pitch, and roll attitudes have steady-state errors of 0.05, 0.3, and 0.02 deg, respectively. These errors occur due to the low sensitivity of the 200-lbf thrusters at very low voltages and pressures.

Conclusions

This paper has successfully demonstrated the application of near-optimal open-loop and Lyapunov closed-loop control methods to maneuver a ground-based model of a spacecraft. The elegant control laws are based on attitude and angular velocity feedback. Torque smoothing was used to minimize high-frequency structural excitations. Accounting for the excessive leakage of the compressed air and its effect on the thruster performance posed the major challenges during the course of this work. The objective of controlling the very low frequency pendulum mode at approximately 0.05 Hz was achieved when enough air pressure was available to drive the thrusters.

Acknowledgments

This research was performed under the NASA-DOD Control-Structure-Interaction Guest Investigator Program (Contract NAS1-19373). Partial support of the Texas Higher Education Coordinating Board through ATP Grant 999903-264 is gratefully acknowledged. The authors are grateful to Alok Das, Kevin Slimack, Sean Curran, and Derek Cossey of the Air Force Phillips Laboratory for their input. Discussions with J. L. Junkins and Thomas Pollock of Texas A&M University have been extremely helpful.

References

[1]Junkins, J. L., and Turner, J. D., *Optimal Spacecraft Rotational Maneuvers*, Elsevier, Amsterdam, 1985.

[2]Scrivener, S., and Thompson, R. C., "Survey of Time-Optimal Attitude Maneuvers," *Journal of Guidance, Control, and Dynamics*, Vol. 17, No. 2, 1994, pp. 225–233.

[3]Abhyankar, N. S., Ramakrishnan, J., Byun, K. W., Das, A., Cossey, D. F., and Berg, J., "Modeling, System Identification and Control of ASTREX," *Proceedings of the 5th NASA/DOD Controls-Structures Interaction Technology Conference* (Lake Tahoe, NV), 1992, pp. 727–739.

[4]Vadali, S. R., Singh, T., and Carter, M. T., "Computation of Near-Minimum-Time Maneuvers of Flexible Structures by Parameter Optimization," *Journal of Guidance, Control, and Dynamics*, Vol. 17, No. 2, 1994, pp. 354–360.

[5]Vadali, S. R., and Junkins, J. L., "Optimal Open loop and Stable Feeback Control of Rigid Spacecraft Attitude Maneuvers," *Journal of the Astronautical Sciences*, Vol. 32, No. 2, 1984, pp. 105–122.

[6]Wie, B., Wiess, H., and Arapostathis, A., "Quaternion Feedback Regulator for Spacecraft Eigenaxis Rotations," *Journal of Guidance, Control, and Dynamics*, Vol. 12, No. 3, 1989, pp. 375–380.

[7]Junkins, J. L., Rahaman, Z., and Bang, H., "Near-Minimum-Time Control of Distributed Parameter Systems: Analytical and Experimental Results," *Journal of Guidance, Control, and Dynamics*, Vol. 14, No. 2, 1991, pp. 406–415.

[8]Vadali, S. R., "Feedback Control of Space Structures: A Lyapunov Approach," *Mechanics and Control of Large Flexible Structures*, edited by J. L. Junkins, Vol. 129, Progress in Astronautics and Aeronautics, AIAA, Washington, DC, 1990, Chap. 24.

[9]Mukherjee, R., and Chen, D., "An Asymptotic Stability Theorem for Autonomous Systems," *Journal of Guidance, Control, and Dynamics*, Vol. 16, No. 5, 1993, pp. 961, 962.

[10]Carter, M. T., Vadali, S. R., and Singh, T., "Near-Minimum-Time Maneuvers of Large Structures Using Parameter Optimization," *Proceedings of the AIAA Guidance, Navigation, and Control Conference* (Monterey, CA), AIAA, Washington, DC, 1993, pp. 127–137 (AIAA Paper 93-3714).

[11]Vadali, S. R., and Carter, M. T., "Near-Minimum-Time Maneuvers of the Advanced Space Structures Technology Experiment (ASTREX) Test Article: Theory and Experiments," NASA CR 4616, Aug. 1994.